Nanocomposites based on nanostructured PI-*b*-PMMA copolymer and selectively placed PMMA-modified magnetic nanoparticles: Morphological and magnetic characterization

I. Barandiaran[1], E. Grana[2,3], D. Katsigiannopoulos[2,3], A. Avgeropoulos[2], G. Kortaberria[1*]

[1]"Materials + Technologies" Group, Universidad del Pais Vasco/Euskal Herriko Unibertsitatea, Plaza Europa 1, 20018 Donostia, Spain

[2]Department of Materials Science and Engineering, University of Ioannina, University Campus - Dourouti, 45110 Ioannina, Greece

[3]Laboratoire de Chimie des Polymères Organiques (LCPO) - UMR5629, Université Bordeaux, CNRS, IPB-ENSCBP, 16 Avenue Pey Berland, 33607 Pessac Cedex, France

*corresponding autor: Galder Kortaberria, Plaza Europa 1, 20018 Donostia, Spain. Tel: 0034 943017176; email: galder.cortaberria@ehu.es

ABSTRACT

Hybrid organic/inorganic nanocomposites with magnetic properties have been prepared, based on nanostructured PI-*b*-PMMA block copolymer and selectively placed magnetic Fe_2O_3 nanoparticles. Magnetic nanoparticles have been functionalized with PMMA brushes by atom transfer radical polymerization in order to increase the compatibility with the PMMA block of the copolymer. The success of nanoparticle modification has been probed by infrared spectroscopy and thermogravimetric analysis. Morphological characterization of the neat block copolymer and the nanocomposites has been studied by small-angle X-ray scattering and atomic force microscopy measurements. For as cast films of nanocomposites, the surface perpendicular lamellar nanostructure was altered with the nanoparticle addition, and a morphology consisting on a mixture of surface parallel and perpendicular lamellae was formed for low nanoparticle amount, while for higher nanoparticle content some cylindrical domains were observed. For films annealed by solvent vapors, the cylindrical morphology of the neat copolymer thin film was maintained for low nanoparticle content, while the ordered morphology was disrupted for the highest nanofiller content. Magnetic characterization by vibrating sample magnetometer and superconducting quantum interference device has demonstrated that magnetic properties of nanoparticles have been transferred to the nanocomposites, exhibiting superparamagnetic behavior similar to that of the maghemite nanoparticles at room temperature.

1. INTRODUCTION

Hybrid nanocomposites based on block copolymer matrices with embedded inorganic nanoparticles have attracted great attention due to their potential in tailoring their properties for numerous applications [1, 2]. The ability of block copolymers to self-

assemble into continuous nanostructures such as lamellar, cylindrical or spherical, among others, makes them excellent candidates for engineering the self-assembly of inorganic nanoparticles within nanodomains, in order to design periodic arrangements for materials with enhanced properties at nanometer scale [3-5]. The addition of functional nanoparticles endows the hybrid nanocomposites with specific advantageous optical, conductive, electric, or magnetic properties [6-8], for various fields of application such as photonic, band gap materials, solar cells, sensors, and high-density magnetic storage devices [1, 9-11]. Several works have been carried out on the preparation of nanocomposites based on block copolymers matrices and magnetic nanoparticles [12-16], in order to prepare hybrid films which can be applied as high density magnetic storage media, thermoresponsive magnetic sensors or drug carriers.

However, when preparing organic-inorganic hybrid nanocomposites the tendency of nanoparticles to aggregate is a big challenge to overcome. Different methods have been used to prevent this problem. For example, Peponi et al. [3] demonstrated that the use of dodecanethiol as surfactant enhanced the dispersion of conductive silver nanoparticles in the desired domains of poly(styrene-*b*-butadiene-*b*-styrene) (SBS) copolymer. Emrick et al [17] controlled the surface hydrophobicity by using different surfactants in order to disperse CdSe nanoparticles in poly(styrene-*b*-2-vinylpiridine) (PS-*b*-P2VP) copolymer, creating hierarchically ordered patterns with CdSe nanoparticles located in the PS or P2VP domains depending on the surfactant. Another common method for dispersing and placing nanoparticles into the desired nanodomain is the growth of polymer brushes on the nanoparticles surface. Different approaches have been used for this purpose such as *grafting to*, *grafting through* and *grafting from*. The control of the functionality, density and molar mass of the polymer brushes is crucial for adequate surface modification. In the first method (*grafting to*) an end-functionalized polymer reacts with the reactive sites on the nanoparticle surface. Our group in previous works [18] used successfully the *grafting to* method to obtain an adequate placement of maghemite nanoparticles on the interfaces of PS-*b*-PCL diblock copolymer [PCL: poly(ε-caprolactone)]. Hailu et al. [19] also used this method to successfully disperse TiO_2 nanoparticles within neat block copolymer thin films. The second method (*grafting through*) consists from a surface polymerization through a covalently linked monomer in which the inorganic phase is incorporated inside the polymer chains. Following this method our group [20] modified semiconductive CdSe nanoparticles with PS polymer brushes, achieving relatively good

placement of the nanoparticles at the PS nanodomains of a SBS triblock copolymer, and also Fe_3O_4 nanoparticles with PMMA brushes in order to be placed at PMMA domains of poly(styrene-*b*-methylmethacrylate) PS-*b*-PMMA copolymer [21]. In the *grafting from* method the polymer chains grow in situ from an initiator that has been previously anchored to nanoparticle surface. The *grafting from* technique results in significantly higher grafting density since the steric barrier towards incoming polymer, imposed by the *in situ* grafted chain does not limit the access of smaller monomer molecules to the active initiation sites [22]. By means of this method Xu et al. [14] modified magnetite nanoparticles with different length PMMA brushes, concluding that the dispersion of the nanoparticles was better when the polymer brushes were the shortest in length. Our group [13] also followed this method to disperse Fe_3O_4 nanoparticles into a P2VP-*b*-PMMA diblock copolymer.

In this work maghemite nanoparticles were modified via atom transfer radical polymerization (ATRP), following the *grafting from* method. PMMA brushes with controlled molar mass were successfully grown from nanoparticle surface. The functionalization of nanoparticles is necessary since it allows their selective placement at PMMA domains for the preparation of hybrid nanocomposites based on maghemite and poly(isoprene-*b*-methylmethacrylate) PI-*b*-PMMA block copolymer. Obtained morphologies and structures were analyzed by atomic force microscopy (AFM) and small-angle X-ray scattering (SAXS) measurements. Magnetic characterization was also carried out in order to check whether the magnetic properties of nanoparticles have been transferred to the nanocomposite films.

2. EXPERIMENTAL

2.1.Materials

PI-*b*-PMMA block copolymer was synthesized through anionic polymerization and sequential addition of monomers under high vacuum conditions. The standards required for anionic copolymerization have been described elsewhere [23]. The block weight ratios were 48 wt% of PI and 52 wt% of PMMA, with Mn_{PI}= 41800 g/mol and Mn_{PMMA}= 48000 g/mol. Maghemite (Fe_2O_3) nanoparticles with a nominal size of 9 nm were purchased from Integram Technologies, Inc. The methyl methacrylate monomer (MMA; 99%) was purchased from Aldrich (Germany) and was distilled under reduced pressure over CaH_2 before use. 2-(4-chlorosulfonylphenyl) ethyltrichlorosilane (CTCS) was purchased from

ABCR (Germany) and used in a 50 wt% solution in dichloromethane, containing 30 wt% of free sulfonic acid and small amounts of silylsulfonic acid, without any further purification. Copper (I) bromide (CuBr; 98.0%), copper (II) bromide ($CuBr_2$; 99.9%), and bipyridine (Bip; 99.0%) were purchased from Aldrich (Germany) and used as received. Hydrofluoric acid (48-51 %) was purchased from Probus.

2.2.Nanoparticle modification

Silanization process

In this work, the immobilization of CTCS initiator on the nanoparticles surface was carried out following the procedure of Marutani et al. [24]. Extra-dry toluene, CTCS, and nanoparticles were mixed in an ultrasonic bath at room temperature. Nanoparticles were subsequently washed with tetrahydrofuran (THF), until any silane rest was eliminated (the presence of silane after washing was probed by FTIR), and then were vacuum dried at 40 ºC for a period of 2 days.

Grafting from polymerization process

The polymerization of MMA was performed with CuBr/bip as catalyst [25, 26] and CTCS on the surface of nanoparticles as initiator. First, CuBr (16.06 mg), $CuBr_2$ (2.35 mg), bip (78.55 mg), and 0.25 g of CTCS-modified nanoparticles were placed in a flask under nitrogen atmosphere and deoxygenated MMA (30 mL) was also added. The flask was then sealed under nitrogen atmosphere and the mixture was left to react under stirring at 70 ºC for 3 h. Nanoparticles were subsequently washed with tetrahydrofuran (THF), until any monomer rest was eliminated (probed by FTIR), and then were vacuum dried at 40 ºC for a period of 2 days. This polymerization conditions were optimized in order to obtain polymer brushes with the desired molar mass, big enough for compatibilization and low enough for the placement of nanoparticles at PMMA domains (as the chains are smaller, wetting of them by PMMA block chains is expected to be better) [14].

Cleavage of PMMA brushes from the nanoparticle surface

In order to characterize the molar mass of PMMA brushes, they were cleavaged from the nanoparticle surface with the following procedure. In a polyethylene flask 100 mg of nanoparticles were inserted together with 3.5 mL of toluene and 3.5 mL of aqueous HF (5 %), and were left to react for 2 h. Then organic and aqueous phases were separated and

the process was repeated at least twice [27]. The separated brushes where analyzed by gel permeation chromatography (GPC).

2.3.Nanocomposite preparation

Nanocomposite thin films were prepared by solvent casting with dichloromethane as solvent. It seems to be adequate for both blocks ($\chi \leq 0.5$ [28]), as χ Flory-Huggins interaction parameters are 0.35 and 0.49 for PI and PMMA, respectively, as obtained from equations 1 and 2.

$$\chi \approx 0{,}34 + \frac{V}{RT}(\delta_P - \delta_S)^2 \quad (1)$$

$$\delta = \sqrt{\frac{E_{coh}}{V}} = \sqrt{\frac{\Delta H_V - RT}{V}} \quad (2)$$

Where χ is the Flory-Huggins interaction parameter, V solvent specific volume, R ideal gas constant, T temperature, δ solubility parameter, E_{coh} cohesive energy and ΔH_V enthalpy of vaporization.

This enables a quick formation of lamellar nanostructure [29]. Nanoparticles were dissolved in dichloromethane by sonication and then PI-*b*-PMMA was added. Solution droplets were placed on a silicon wafer and maintained at room temperature until complete solvent removal. Nanocomposites with nanoparticle amounts from 0.1 to 5 wt% were prepared.

The effect of solvent vapor annealing on the adopted morphologies was also analyzed. For this purpose, films obtained for solvent casting were placed in a 250 mL flask with 10 mL of acetone at room temperature for 96 h. Acetone is a selective solvent for PMMA (Flory-Huggins interaction parameters of 0.50 and 0.92 for PMMA and PI, respectively, as obtained from equations 1 and 2).

2.4.Characterization techniques

FTIR was carried out with a Nicolet Nexus 600 FTIR spectrometer, performing 20 scans with a resolution of 4 cm^{-1}.

TGA was performed with a Mettler Toledo TGA/SDTA851 instrument. Tests were carried out from room temperature to 750 ºC with a heating rate of 10 ºC/min.

Surface morphologies obtained for different films were studied by AFM with a scanning probe microscopy instrument AFM Dimension ICON by Bruker, operating in tapping mode (TM-AFM). An integrated silicon tip/cantilever, from the same manufacturer, having a resonance frequency of around 300 kHz, was used. Measurements were performed at a scan rate of 1 Hz/s, with 512 scan lines.

SAXS measurements were performed on a Ganesha 300XL SAXS-WAXS system (SAXSLAB ApS, Copenhagen/ Denmark) equipped with a GENIX 3D microfocus X-ray source and optic, a three-(scatterless)-slit collimation system, a fully evacuated sample chamber and beam path, and a movable two-dimensional (2D) Pilatus 300 K detector. Samples on mica were measured at room temperature.

Magnetic measurements were performed with SQUID magnetometer and VSM. The SQUID magnetometer (MPMS-7T, Quantum Design) has a superconducting magnet of 7 T, it was used to obtain the ZFC and FC curves. The VSM (CFMS, Cryogenic Ltd) has a superconducting magnet of 14 T.

3. RESULTS AND DISCUSSION

3.1.Iron oxide nanoparticle silanization

Nanoparticles were surface-modified with CTCS silane, since its sulfonyl chloride groups will allow the growth of PMMA chains from the surface [26]. The success of the silanization process has been studied by FTIR and TGA measurements, as it can be seen in Figure 1. CTCS is bonded to the nanoparticle through the hydroxyl groups at the surface. In the FTIR spectra (Figure 1A) characteristic bands related to CTCS can be seen: the stretching vibration of the sulfonyl group at 1406 and 1174 cm^{-1} and the stretching vibration of Fe-O-Si bond at 1121 cm^{-1}. TGA thermogram (Figure 1B) also shows the presence of CTCS at the surface and has been used to calculate the amount of grafted silane [30]. Before calculating the amount of grafted silane, hydroxyl density should have been calculated. The weight loss of the unmodified nanoparticles is related to physisorbed water and the hydroxyl groups present at their surface. The physisorbed water is lost between 25 and 150 °C, while the hydroxyl groups are degraded between 150 and 750 °C [31]. To calculate the hydroxyl density the weight loss of pristine nanoparticles between 150 and 750 ºC should be taken into account, accompanied with the specific surface area value (123 m^2/g, calculated by BET). The hydroxyl surface density was calculated to be 8.1 OH/nm^2 and the calculated surface density of the initiator 1.1 $molecules/nm^2$;

therefore the yield of the silanization process was calculated approximately to be equal to 13 %.

3.2.PMMA brush synthesis by ATRP

The growth of PMMA brushes from the surface of maghemite nanoparticles was also verified by FTIR and TGA studies. In the FTIR spectra of Figure 1A bands related with PMMA can be seen: C=O stretching vibration at 1703 cm^{-1} and C-O-C stretching deformation vibration at 1237 cm^{-1}. The presence of bands related to the methacrylate group confirmed that the polymerization of PMMA brushes was carried out successfully. The grafting density of polymer brushes was calculated directly from the weight loss of TGA thermogram (Figure 1B) according to the method used by Cosio-Castañeda et al. [31], obtaining a value of 0.8 chains/nm^2. This grafting density value is in the order of those calculated by other authors [32] following the same method. Moreover, if this grafting density value is compared to that obtained in our previous work by the *grafting to* method (0.04 chains/nm^2) [18], the increase of density maybe attributed to the ATRP method adopted for the polymer brush synthesis. According to Ferreira et al. [33], as $\sigma\sqrt{N} > 1$, where N is the number of monomers in the chains and σ the grafting density, nanoparticles are functionalized by dense brushes. Brushes of approximately 1000 g/mol were obtained, as measured by GPC after cleavage. As mentioned above, the polymerization process was previously optimized in order to obtain short brushes which lead to better dispersion within the PMMA domains of the copolymer [14].

3.3.Morphological characterization of nanocomposites based on PI-*b*-PMMA and modified nanoparticles

Morphological characterization of both as cast and solvent annealed nanocomposite films was carried out by SAXS and AFM measurements.

3.3.1. As cast nanocomposites

In Figure 2 AFM phase images of as cast nanocomposite films can be seen, together with that of neat copolymer. For the neat diblock copolymer, regular lamellar morphology with lamellae perpendicular to the surface can be easily seen from the AFM phase image (Figure 2A), but when nanoparticles are added the orientation of lamellae changes, resulting in a mixture of perpendicular and parallel lamellae [34]. This could be due to nanoparticle addition that could modify the interaction between block copolymer domains

and the substrate, evolving an orientation change of the lamellar nanostructure [35, 36]. For the highest nanoparticle concentration some cylinder forming structures appear between the PMMA lamellae, probably be due to the placement of the PMMA functionalized nanoparticles within the PMMA domains that could lead to an increase of the volume fraction of PMMA domains, the system undergoing a transition from lamellar to cylindrical morphology [37].

3.3.2. Solvent vapor annealed nanocomposites

As it was previously mentioned, nanocomposites were also annealed in acetone vapors. Acetone is a selective solvent for the PMMA block, and as it was shown in our previous work, when PI-*b*-PMMA block copolymer is placed into acetone environment its nanostructure changes from lamellar to cylindrical [29]. If a block copolymer thin film is exposed to a solvent selective for one of the blocks, the nanostructure is enhanced significantly, and a long-range orientation order is achieved [38]. In Figure 3 the SAXS patterns of as cast neat block copolymer film can be seen. The first order peak is at q_1= 0.0121 nm^{-1} and the third order peak at $q_3 = 3 \cdot q_1$ = 0.0363 nm^{-1}, indicative of lamellar nanostructure [39]. Furthermore, the lack of the second order peak is attributed to the almost symmetric volume fractions (*f*) leading to zero intensity when *n = 2*, according to the following equation from which the intensity of each permitted reflection is calculated for alternating lamellae morphology in a SAXS pattern:

$$I_n \sim \left(\frac{sin(nf\pi)}{n}\right)^2 \quad (3)$$

On the other hand, the solvent vapor annealed neat diblock copolymer first order peak is at q_1= 0.0072 nm^{-1}, second order peak at $q_2 = \sqrt{3} \cdot q_1$= 0.0108 nm^{-1} and fourth order peak at $q_4 = \sqrt{7} \cdot q_1$= 0.0252 nm^{-1}, which is consistent with the permitted reflections ratio for a hexagonally packed cylindrical nanostructure [40].

As it can be seen in the AFM phase images of Figure 4 the cylindrical morphology obtained for the neat diblock copolymer after solvent annealing (Figure 4A) is maintained for nanocomposites with 0.1, 1, and 2 wt% nanoparticles (Figure 4B, 4C and 4D, respectively), even if some small defects are evident in the nanostructure probably due to the presence of nanoparticles. For the nanocomposite with the highest nanoparticle content (5 wt%) (Figure 4E), the cylindrical nanostructure is disrupted and disordered morphology is obtained. The addition of fillers to the block copolymer and the solvent

treatment can modify the order-disorder transition temperature of a block copolymer [41, 42]. These facts could be the reason of reaching disordered state with 5 wt% of nanoparticles after exposure to acetone, the combined effect of the nanoparticles and solvent exposure could facilitate that the system reaches disordered state more easily.

3.3.3. Degradation by UV light irradiation

In order to better visualize the location of the maghemite nanoparticles on the nanostructures, the organic part of the as cast nanocomposites was removed by exposure to UV light irradiation [43, 44]. Figure 5 shows AFM phase images of neat copolymer films exposed to UV light for different times. PMMA block domains are degraded first. When the copolymer is exposed to UV light irradiation for 6 h (Figure 5B) the lamellar nanostructure of the film is maintained, although the height profile of the copolymer is smoother, indicating that the PMMA block has degraded more than the PI segments. By exposing the copolymer for 48 hours (Figure 5C) the nanostructure totally disappears and both blocks are degraded. When UV light irradiation is applied to the nanocomposites the organic part is removed, leaving the iron oxide nanoparticles on the silicon surface. Figure 6 shows the AFM phase images for the nanocomposite with 1 wt% nanoparticles as an example, after 48 h of exposure to UV light. As it can be seen, nanoparticles with quite homogeneous size are well dispersed in the nanocomposite. If we compare the AFM phase image of the nanocomposites with 1 wt% of nanoparticles and the AFM image of the iron oxide nanoparticles after removing the block copolymer matrix by UV light irradiation (superposition of images shown in Figure 7), it can be concluded that the position of the nanoparticles coincides almost totally with the PMMA domains, suggesting that the iron oxide nanoparticles are located within the PMMA domains of the block copolymer matrix, due to their functionalization with PMMA brushes.

3.4.Magnetic characterization

In order to magnetically characterize the nanocompostites, both zero-field-cooled/field-cooled (ZFC/FC) curves and M *vs* B (B applied magnetic field, M induced magnetic moment) measurements have been carried out by SQUID. In Figure 8 ZFC/FC curves of as cast nanocomposite films with 2 and 5 wt% of nanoparticles can be seen. Both samples exhibit a typical superparamagnetic behavior at room temperature and ferromagnetic one at low temperatures [45-47]. Below the blocking temperature (T_b) the field-cooled (FC) and zero-field-cooled (ZFC) magnetization curves diverge, magnetic moment are

singledomain, pinned by anisotropy at low temperature and thermally disordered above the blocking temperature. If the results obtained from the nanocomposites with 2 and 5 wt% of nanoparticles are compared, it can be seen that the T_b is higher when the nanoparticle concentration is higher. As the T_b is related to the size of nanoparticle, or formed aggregates, it seems that for higher nanoparticle concentration bigger aggregates are formed.

Apart from FC/ZFC curves the hysteresis loops were also measured at different temperatures of 2, 50 and 150 K (Figure 9) with VSM. Below the blocking temperature the hysteresis loops are hysteretic while appear as non-hysteretic above the T_b. In the M *vs* B magnetization curve at 2 K the hysteresis is observed with a coercivity of approximately 300 Oe and a remanence of $1.5 \cdot 10^{-5}$ emu, whereas above the T_b both the coercivity and remanence are zero, demonstrating the superparamagnetic behavior of the final nanocomposites [35, 48]. This superparamagnetic behavior was detected for all the nanocomposites prepared.

4. CONCLUSIONS

In this work we have demonstrated that the *grafting from* technique is an adequate method to modify nanoparticles increasing their compatibility with a copolymer, in order to increase their dispersion within the desired domains (PMMA ones in this case). Successful grafting of PMMA brushes from the nanoparticle surface with a grafting density of 0.8 chain/nm^2 has been achieved. This functionalization of the nanoparticle surface enables a good dispersion of nanoparticles in the polymeric matrix and also their placement within the PMMA domains. Morphological changes promoted by solvent treatment and nanoparticle addition have been studied. For as cast films, nanoparticle addition provokes a morphological change even for low nanoparticle amount, provoking a change in the orientation of lamellae, and, for the highest content, also the formation of some cylinders. For solvent annealed nanocomposites, the nanostructure of neat copolymer is maintained up to 2 wt% of nanoparticles. The selective location of well dispersed nanoparticles within the PMMA domains was corroborated removing the organic part of the nanocomposites by exposure to UV light irradiation. Through magnetic measurements the relevant magnetic properties of the nanocomposites were verified, concluding that magnetic properties of nanoparticles were transferred to the nanocomposites.

AKNOWLEDGEMENTS

Financial support from the Basque Country Government (Grupos Consolidados, IT-776-13) and the Ministry of Economy and Competitiveness (MAT 2012-31675) is gratefully acknowledged. The technical and human support provided by SGIker of UPV/EHU is also acknowledged. I.B. thanks Euskal Herriko Unibertsitatea/Universidad del País Vasco for Ph.D Fellowship (Becas de Formación de Investigadores 2011 (PIF/UPV/11/030)).

REFERENCES

[1] Bockstaller M.R., Mickiewicz R.A., Thomas E.L., Block copolymer nanocomposites: perspectives for tailored functional materials. *Adv. Mater*. 2005, 17, 1331-1349. Doi: 10.1002/adma.200500167.

[2] Lazzari M., López-Quintela M.A., Block copolymers as a tool for nanomaterial fabrication. *Adv. Mater*. 2003, 15, 1583-1594. Doi: 10.1002/adma.2003.

[3] Peponi L., Tercjak A., Gutierrez J., Stadler H., Torre L., Kenny J. M., Mondragon I., Self assembly of SBS copolymers as templates for conductive silver nanocomposites. *Macromol Matert Eng* 2008, 293, 568-573. Doi: 10.1002/mame.200800033

[4] Lo C.T., Lee B., Winans R.E., Thiyagarajan P., Effect of dispersion of inorganic nanoparticles on the phase behavior of block copolymers in selective solvent. *Macromolecules* 2006, 39, 6318-6320. Doi: 10.1021/ma060879o

[5] Lin Y., Boker A., He J., Sill K., Xiang H., Abetz C., Li X., Wang J., Balazs A., Russel T.P., Self-directed self-assembly of nanoparticle/block copolymer mixtures. *Nature* 2005, 434, 55-59. Doi: 10.1038/nature03310

[6] Gutierrez J., Tercjak A., Peponi L., Mondragon I., Conductive Properties of Inorganic and Organic TiO_2/Polystyrene-block-Poly(ethylene oxide) Nanocomposites. *J. Phys. Chem. C* 2009, 113, 8601-8605. Doi: 10.1021/jp900858f

[7] Etxeberria H., Tercjak A., Mondragon I., Eceiza A., Kortaberria G., Electrostatic force microscopy measurements of CdSe-PS nanoparticles and CdSe-PS/poly(styrene-b-butadiene-b-styrene) nanocomposites. *Collod Polym Sci* 2014, 292, 229-234. Doi: 10.1007/s00396-013-3061-3

[8] Xia X., Metwalli E., Ruderer M.A., Körstgens V., Busch P., Böni P., Müller-Buschbaum P., Nanostructured diblock copolymer films with embedded magnetic nanoparticles. *J. Phys.: Condens. Matter* 2011, 23, 254203 (9pp). Doi: 10.1088/0953-8984/23/25/254203

[9] Park S., Lee D.H., Xu J., Kim B., Hong S.W., Jeong U., Xu T., P. Russell T.P., Macroscopic 10-Terabit–per– Square-Inch Arrays from Block Copolymers with Lateral Order. *Science* 2009, 323, 1030-1033. Doi: 10.1126/science.1168108

[10] Jang Y.H., Xin X., Byun M., Jang Y.J., Lin Z., Kim D.H., An Unconventional Route to High-Efficiency Dye-Sensitized Solar Cells via Embedding Graphitic Thin Films into TiO_2 Nanoparticle Photoanode. *Nano Lett.* 2012, 12, 479-485. Doi: 10.1021/nl203901m

[11] Darling S.B., Yufa N.A., Cisse A.L., Bader S.D., Sibener S.J., Self-organization of FePt nanoparticles on photochemically modified diblock copolymer templates. *Adv. Mater.* 2005, 17, 2446-2450. Doi: 10.1002/adma.200500960

[12] Yao Y., Metwalli E., Su B., Körstgens V., Moseguí González D., Miasnikova A., Laschewsky A., Opel M., Santoro G., Roth S.V., Müller-Buschbaum P., Arrangement of Maghemite Nanoparticles via Wet Chemical Self-Assembly in PS-*b*-PNIPAM Diblock Copolymer Films. *Appl. Mater. Interfaces* 2015, 7, 13080 − 13091. Doi: 10.1021/acsami.5b03308

[13] Garcia I., Tercjak A., Gutierrez J., Rueda L., Mondragon I., Nanostructuration via Solvent Vapor Exposure of Poly(2-vinyl pyridine-b-methyl methacrylate) Nanocomposites Using Modified Magnetic Nanoparticles. *J. Phys. Chem. C* 2008, 112, 14343-14347. Doi: 10.1021/jp802345q

[14] Xu C., Ohno K., Ladmiral V., Composto R.J., Dispersion of polymer grafted magnetic nanoparticles in homopolymers and block copolymers. *Polymer* 2008, 49, 3568-3577. Doi: 10.1016/j.polymer.2008.05.040

[15] Wu J., Li H., Wu S., Huang G., Xing W., Tang M., Fu Q., Influence of Magnetic Nanoparticle Size on the Particle Dispersion and Phase Separation in an ABA Triblock Copolymer. *J. Phys. Chem. B* 2014, 118, 2186-2193. Doi: 10.1021/jp410604a.

[16] Lu W., Shen Y., Xie A., Zhang W., Preparation and drug-loading properties of Fe_3O_4/Poly(styrene-co-acrylicacid) magnetic polymer nanocomposites. *Journal of Magnetism and Magnetic Materials* 2013, 345, 142-146. Doi: 10.1016/j.jmmm.2013.06.020

[17] Zou S., Hong R., Emrick T., Walker G. C., Ordered CdSe nanoparticles within self-assembled block copolymer domains on surfaces. *Langmuir* 2007, 23, 1612-1614. Doi: 10.1021/la0629274

[18] Barandiaran I., Cappelletti A., Strumia M., Eceiza A., Kortaberria G., Generation of nanocomposites base on (PMMA-*b*-PCL) grafted Fe_2O_3 nanoparticles and PS-*b*-PCL nanoparticles. *European Polymer Journal* 2014, 58, 226-232. Doi: 10.1016/j.eurpolymj.2014.06.022

[19] Hailu S.T., Samant S., Grabowski C., Durstock M., Karim A., Raghavan D., Synthesis of highly dispersed, block copolymer-grafted TiO_2 nanoparticles within neat block copolymer films. *Journal of Polymer Science Part A* 2015, 53, 468-478. Doi: 10.1002/pola.27460

[20] Etxeberria H., Zalakain I., Mondragon I., Eceiza A., Kortaberria G., Generation of nanocomposites based on polystyrene-grafted CdSe nanoparticles by grafting through and block copolymer. *Colloid Polym Sci* 2013, 291, 1881-1886. Doi: 10.1007/s00396-013-2927-8

[21] Barandiaran I., Kortaberria G., Selective placement of magnetic Fe_3O_4 nanoparticles into the lamellar nanostructure of PS-b-PMMA diblock copolymer. *European Polymer Journal* 2015, 68, 57-67. Doi: 10.1016/j.eurpolymj.2015.04.034

[22] Radhakrishnan B., Ranjan R., Brittain W.J., Surface initiated polymerizations from silica nanoparticles. *Soft Matter* 2006, 2, 386–396. Doi: 10.1039/B516508C

[23] Litina K, Miriouni A, Gournis D, Karakassides M, Georgiou N, Klontzas E, Ntoukas E Avgeropoulos A., Nanocomposites of polystyrene-*b*-polyisoprene copolymer with layered silicates and carbon nanotubes. *Eur Polym J* 2006, 42, 2098-2107. Doi: 10.1016/j.eurpolymj.2006.03.025.

[24] Marutani E., Yamamoto S., Ninjbadgar T., Tjii Y., Fukuda T., Takano M., Surface-initiated atom transfer radical polymerization of methyl methacrylate on magnetite nanoparticles. *Polymer* 2004, 45, 2231 − 2235. Doi: 10.1016/j.polymer.2004.02.005

[25] Wang, J.; Matyjaszewski, K., Controlled/"Living" Radical Polymerization. Halogen Atom Transfer Radical Polymerization Promoted by a Cu(I)/Cu(II) Redox Process. *Macromolecules* 1995, 28, 7901−7910. Doi: 10.1021/ma00127a042

[26] García I., Zafeiropoulos N.E., Janke A., Tercjak A., Eceiza A., Stamm M., Mondragon I., Functionalization of Iron Oxide Magnetic Nanoparticles with Poly(methyl methacrylate) Brushes Via Grafting-From Atom Transfer Radical Polymerization. *Journal of Polymer Science: Part A: Polymer Chemistry* **2007**, 45, 925-932. Doi: 10.1002/pola.21854

[27] Lan Q., Francis L.F., Bates F.S., Silica Nanoparticle Dispersions in Homopolymer Versus Block Copolymer. *Journal of Polymer Science: Part B: Polymer Physics* 2007, 45, 2284-2299. Doi: 10.1002/polb.21251

[28] Van Krevelen D.W., Properties of Polymers. Elsevier Scientific Publishing Sons,1989, New York

[29] Barandiaran I., Katsigiannopoulos D., Grana E., A. Avgeropoulos A., Eceiza A., Kortaberria G., PI-*b*-PMMA diblock copolymers: nanostructure development in thin films and nanostructuring of thermosetting epoxy systems. *Colloid Polym Sci* 2013 291, 2173–2180. Doi: 10.1007/s00396-013-2961-6

[30] Bartholome C., Beyou E., Bourgeat-Lami E., Chaumont P., Zydowicz N., Nitroxide-Mediated Polymerizations from Silica Nanoparticle Surfaces: "Graft from" Polymerization of Styrene Using a Triethoxysilyl-Terminated Alkoxyamine Initiator. *Macromolecules* 2003, 36, 7946-7952. DOI: 10.1021/ma034491u

[31] Cosio-Castañeda C., Martinez-Garcia R., Socolovsky L.M., Synthesis of silanized maghemite nanoparticles onto reduced graphene sheets composites. *Solid State Sci* 2014, 30, 17-20. Doi: 10.1016/j.solidstatesciences.2014.02.004

[32] Ohno K., Morinaga T., Koh K., Tsujii Y., Fukuda T., Synthesis of Monodisperse Silica Particles Coated with Well-Defined, High-Density Polymer Brushes by Surface-Initiated Atom Transfer Radical Polymerization. *Macromolecules* 2005, 38, 2137-2142. Doi: 10.1021/ma048011q

[33] Ferreira P.G., Ajdari A., Leibler L., Scaling Law for Entropic Effects at Interfaces between Grafted Layers and Polymer Melts. *Macromolecules* 1998, 31, 3994-4003. Doi: 10.1021/ma9712460

[34] Deshmukh R.D., Buxton G.A., Clarke N., Composto R.J., Nanoscale Block Copolymer Templates Decorated by Nanoparticle Arrays. *Macromolecules* 2007, *40,* 6316-6324. Doi: 10.1021/ma0707943

[35] Xu C., Ohno K., Ladmiral V., Milkie D.E., Kikkawa J.M., Composto R.J., Simultaneous Block Copolymer and Magnetic Nanoparticle Assembly in Nanocomposite Films. *Macromolecules* 2009, 42, 1219-1228. Doi: 10.1021/ma8022266

[36] Yoo M., Kim S., Jang S.G., Choi S.-H., Yang H., Kramer E.J., Lee W.B., Kim B.J., Bang J., Controlling the Orientation of Block Copolymer Thin Films using Thermally-Stable Gold Nanoparticles with Tuned Surface Chemistry. *Macromolecules* 2011, 44, 9356-9365. Doi: 10.1021/ma2019254

[37] Lo C.-T., Lee B., Pol V.G., Dietz Rago N.L., Seifert S., Winans R.E., Thiyagarajan P., Effect of Molecular Properties of Block Copolymers and Nanoparticles on the Morphology of Self-Assembled Bulk Nanocomposites. *Macromolecules* 2007, 40, 8302-8310. Doi: 10.1021/ma070835v

[38] Park S., Kim B., Xu J., Hofmann T., Ocko B.M., Russell T.P., Lateral Ordering of Cylindrical Microdomains Under Solvent Vapor. *Macromolecules* 2009, 42, 1278-1284. Doi: 10.1021/ma802480s

[39] Porto L.C., Aissou K., Giacomelli C., Baron T., Rochas C., Pignot-Paintrand I., Armes S.P., Lewis A.L., Soldi V., Borsali R., Nanostructured Films Made from Zwitterionic Phosphorylcholine Diblock Copolymer Systems. *Macromolecules* 2011, 44, 2240-2244. Doi: 10.1021/ma1029554

[40] Li H., Gu W., Zhang Y., Russel T.P., Coughlin E.B., Synthesis of Semicrystalline/Fluorinated Side-Chain Crystalline Block Copolymers and Their Bulk and Thin Film Nanoordering. *Macromolecules* 2013, 46, 3737-3745. Doi: 10.1021/ma400533w

[41] Zhao Y., Saijo K., Takenaka M., Koizumi S., Hashimoto T., Order-Disorder Transition of Nanocomposites: Pd Nanoparticles in Polystyrene-block-Polyisoprene Microdomain Templates. *Macromolecules* 2009, 42, 5272-5277. Doi: 10.1021/ma900342v

[42] Hanley K.J., Lodge T.P., Huang C.-I., Phase Behavior of a Block Copolymer in Solvents of Varying Selectivity. *Macromolecules* 2000, 33, 5918-5931. Doi: 10.1021/ma000318b

[43] Peng J., Knoll W., Park C., Kim D.H., Two-Dimensional Arrays of Strings of TiO_2 Nanoparticles via Cooperative Block Copolymer Self-Assembly. *Chem. Mater.* 2008, 20, 1200-1202. Doi: 10.1021/cm7026042

[44] Gutierrez J., Tercjak A., Garcia I., Mondragon I., The effect of thermal and vapor annealing treatments on the self-assembly of TiO_2/PS-*b*-PMMA nanocomposites generated via the sol-gel process. *Nanotechnology* 2009, 20, 225603 (9pp). Doi: 10.1088/0957-4484/20/22/225603

[45] Chitu L., Jergel M., Majkova E., Luby S., Capek I., Satka A., Ivan J., Kovac J., Timko M., Structure and magnetic properties of $CoFe_2O_4$ and Fe_3O_4 nanoparticles. *Materials Science and Engineering C* 2007, 27, 1415-1417. Doi: 10.1016/j.msec.2006.07.036

[46] Zeng H., Black C.T., Sandstrom R.L., Rice P.M., Murray C.B., Sun S., Magnetotransport of magnetite nanoparticle arrays. *Physical Reviw B* 2006, 73, 020402(R). Doi:10.1103/PhysRevB.73.020402

[47] Bean C.P., Livingston J.D., Superparamagnetism. *J. Appl. Phys.* 1959, 30, S120. Doi: 10.1063/1.2185850

[48] Schulz L., Schirmacher W, Omran A., Shah V.R., Böni P., Petry W., Müller-Buschbaum P., Elastic torsion effects in magnetic nanoparticle diblock-copolymer structures. *J. Phys.: Condens. Matter* 2010, 22, 346008 (6pp). Doi: 10.1088/0953-8984/22/34/346008

FIGURE AND SCHEME CAPTIONS

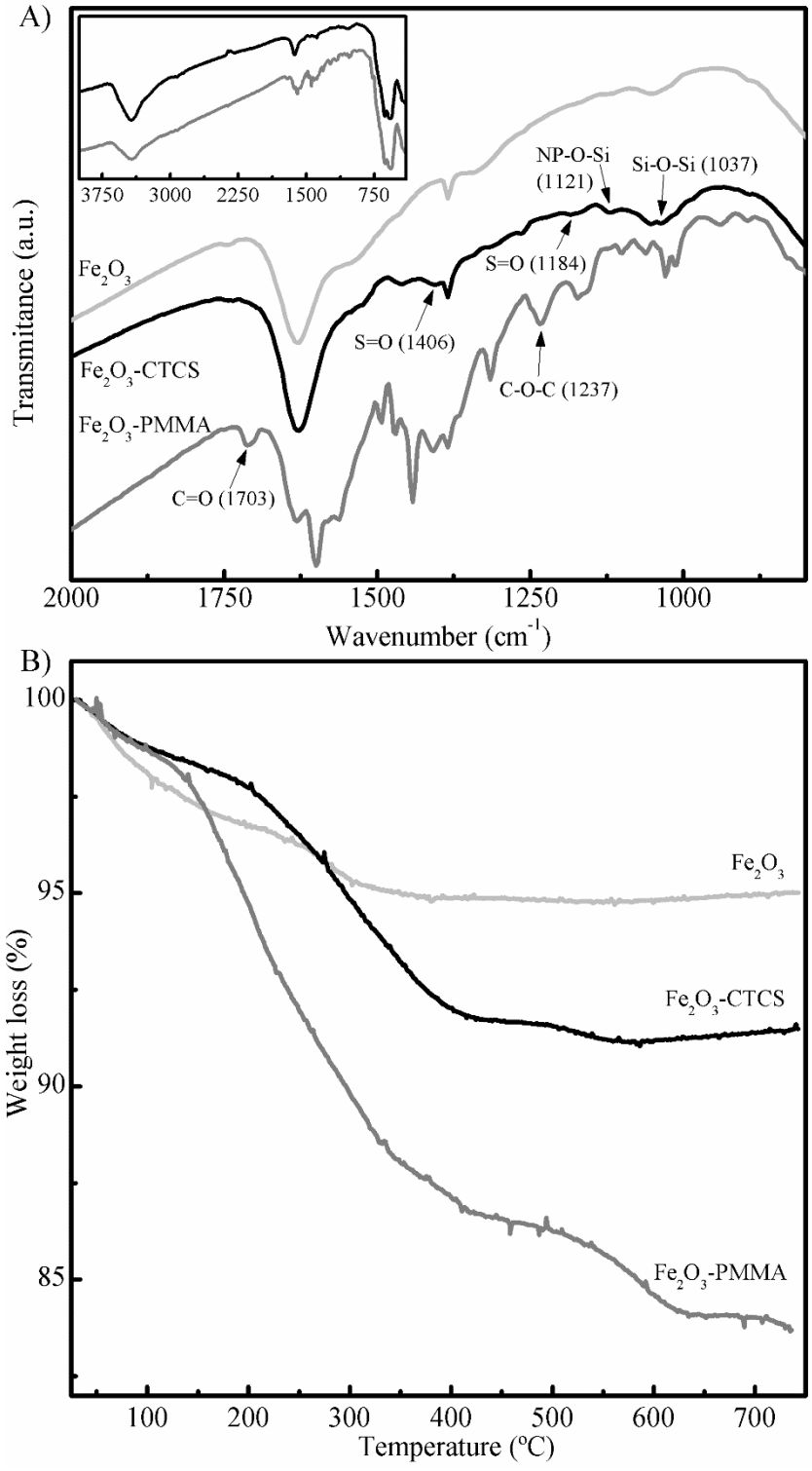

Figure 1. A) FTIR spectra of silanized and PMMA-modified nanoparticles. Inner spectrum shows a magnification of modified nanoparticle spectrum. B) TGA thermogram of neat, silanized, and PMMA-modified Fe_2O_3 nanoparticles.

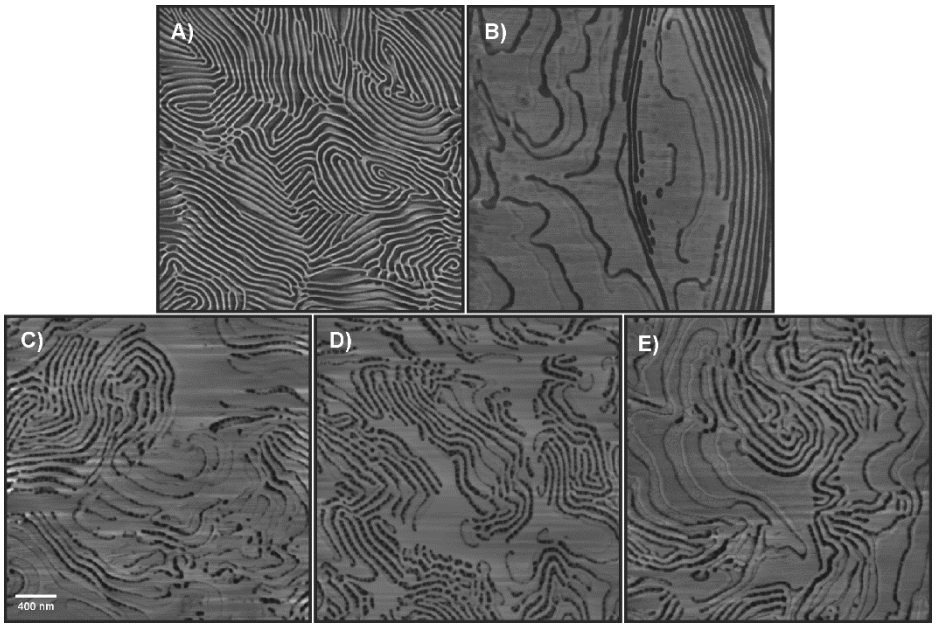

Figure 2. AFM phase images of as cast A) neat block copolymer and nanocomposite films with B) 0.1, C) 1, D) 2 and E) 5 wt% of nanoparticles

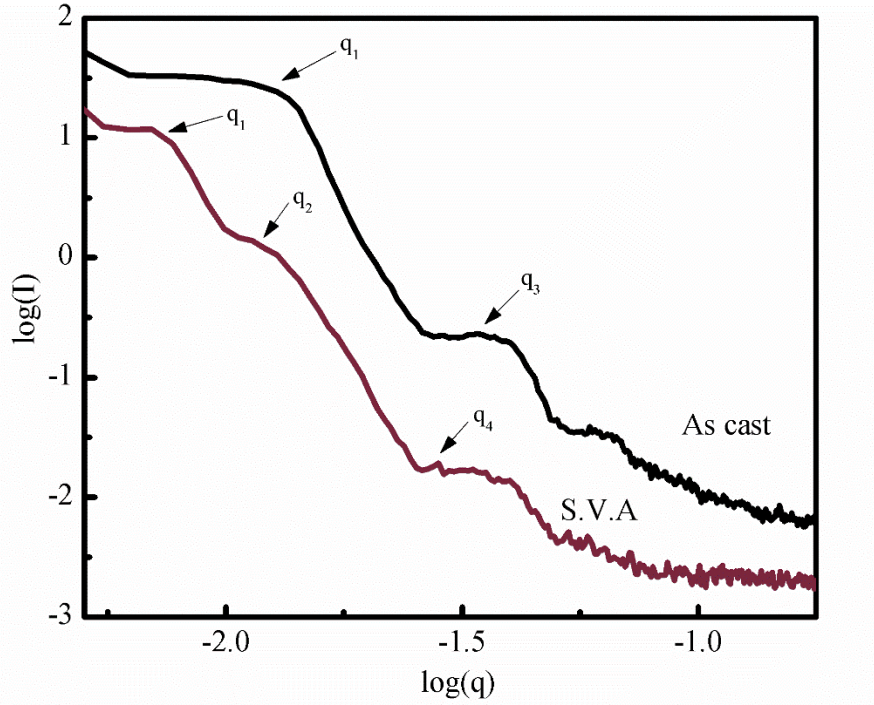

Figure 3. SAXS patterns of neat block copolymer and solvent vapor annealed samples

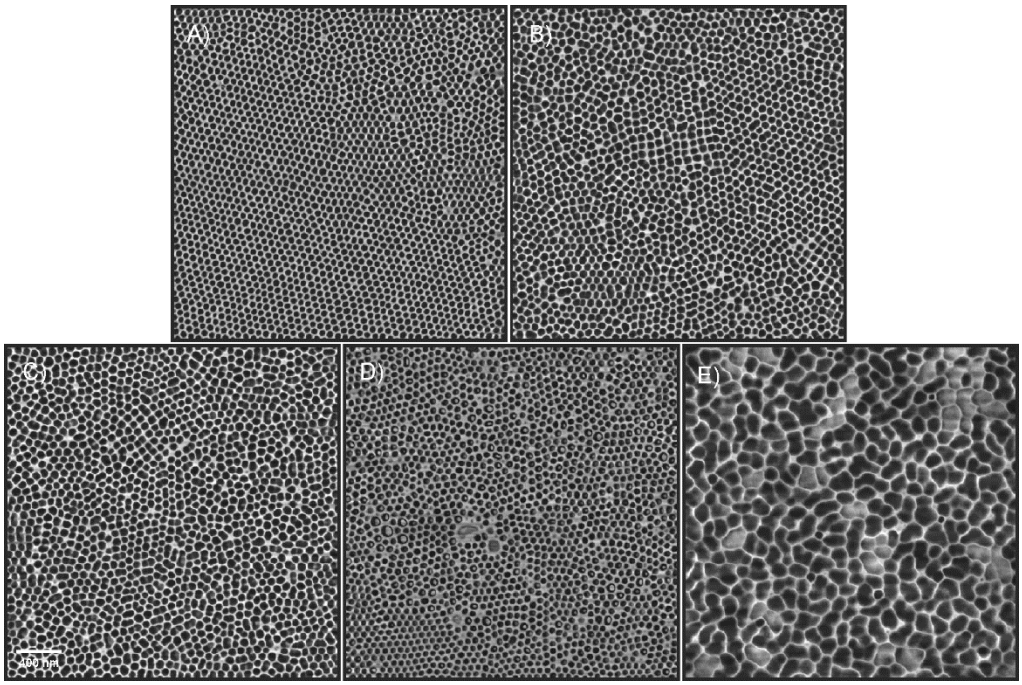

Figure 4. AFM phase images of A) neat block copolymer and nanocomposite films with B) 0.1, C) 1, D) 2 and E) 5 wt% of nanoparticles, annealed under acetone vapors solvent for 96 h

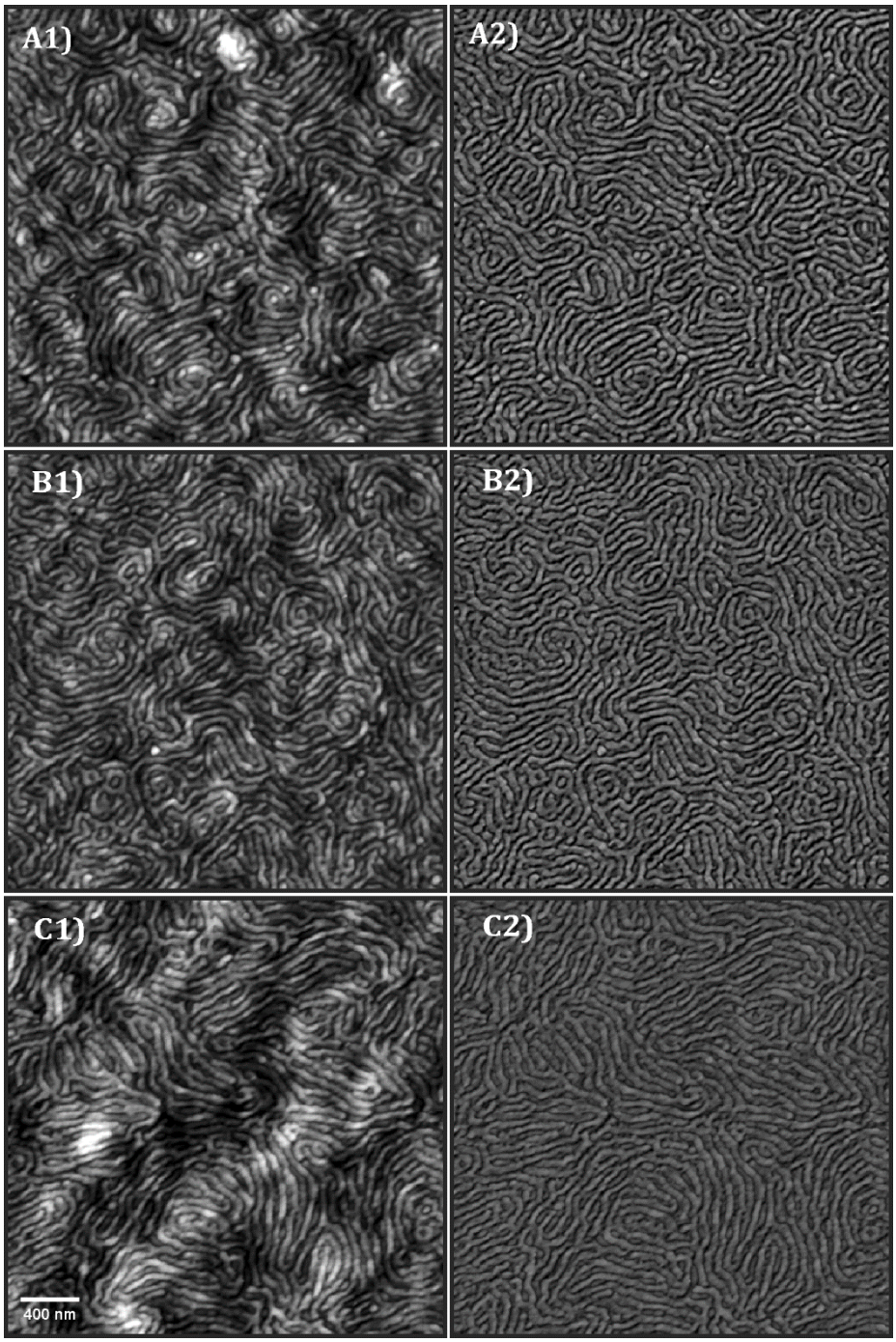

Figure 5. AFM phase, 3D height and profile images of A) neat block copolymer, B) neat block copolymer exposed to UV light irradiation for 6 h and C) neat block copolymer exposed to UV light irradiation for 48 h.

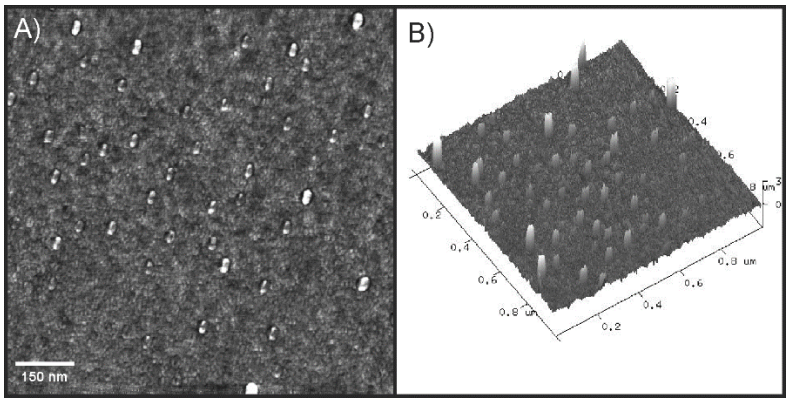

Figure 6. AFM phase and 3D height images of nanocomposite with 1 wt% of nanoparticles exposed to UV light irradiation for 48 h.

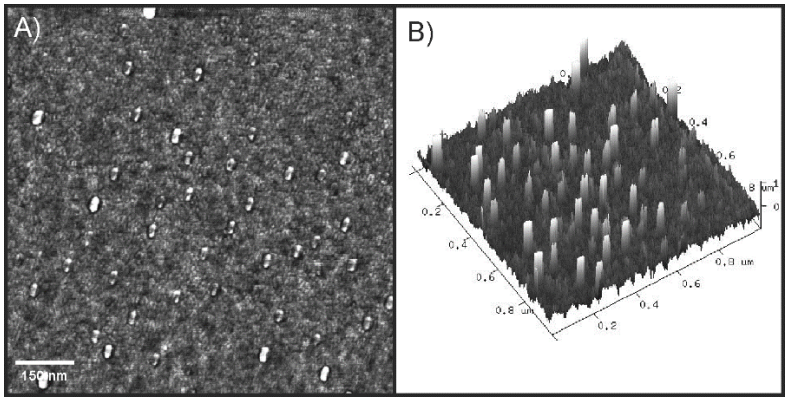

Figure 7. A) AFM phase image of as cast nanocomposite films with 1 wt% of nanoparticles, B) AFM phase image of nanocomposite film with 1 wt% of nanoparticles exposed to UV light irradiation for 48 h, C) superposition of figures 7A and 7B.

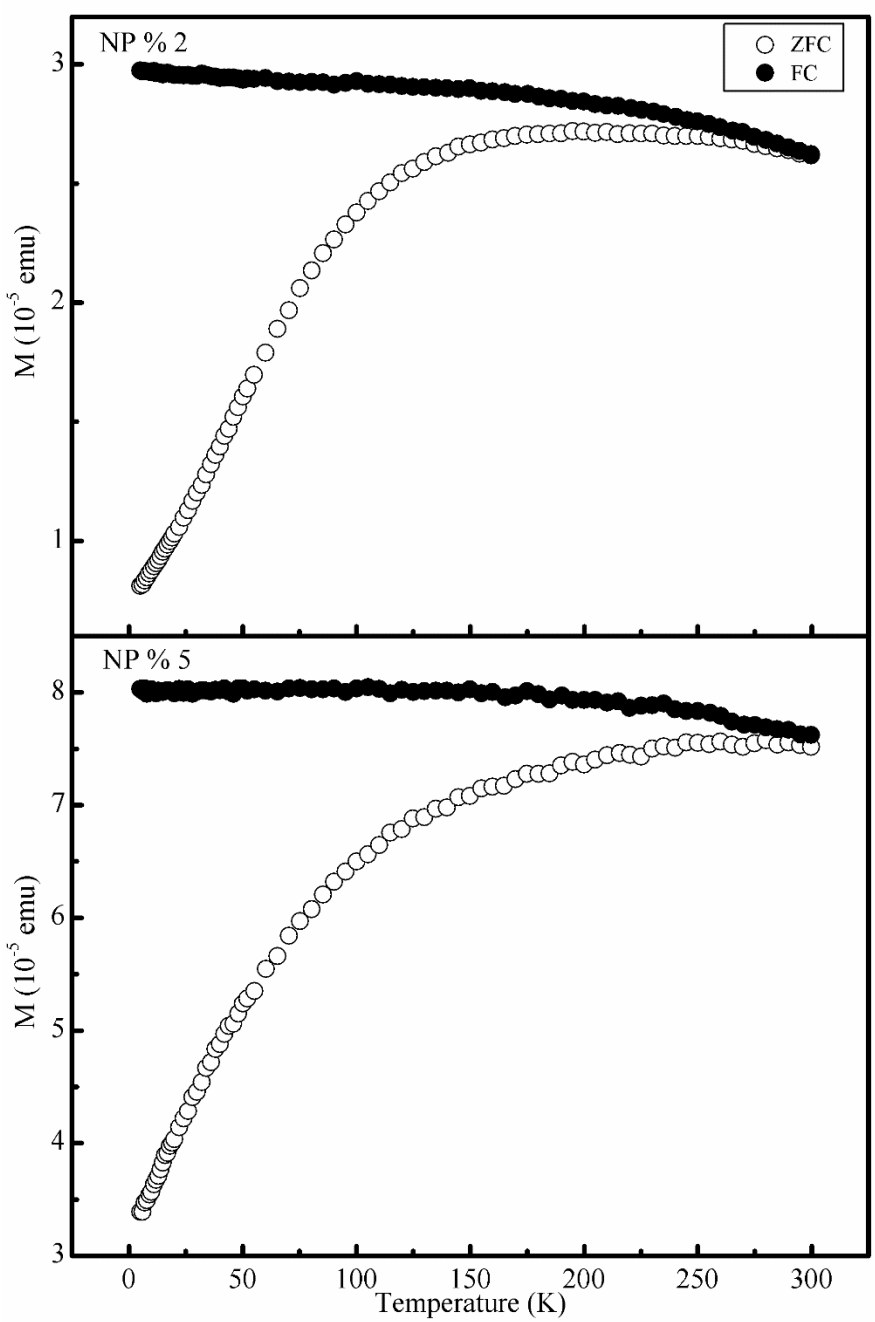

Figure 8. ZFC and FC curves at 100 Oe for as cast nanocomposites with 2 and 5 wt% of nanoparticles

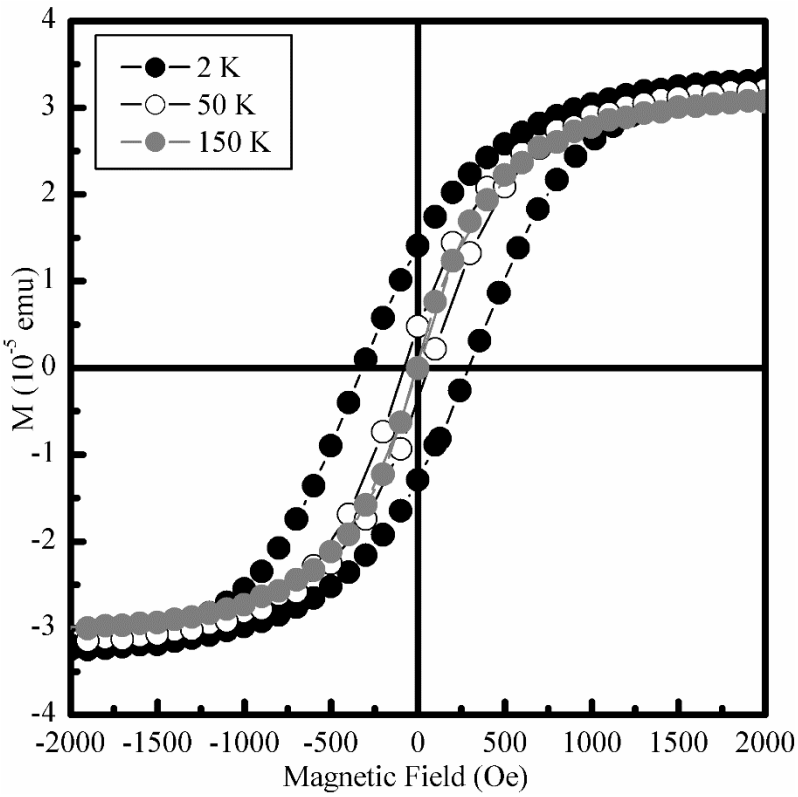

Figure 9. M *vs* B curves at 2, 5 and 150 K for the as cast nanocomposite with 5 wt% of nanoparticles